Ultrahigh-*Q* Resonance in Bound States in the Continuum–Enabled Plasmonic Terahertz Metasurface

Md Saiful Islam,* Aditi Upadhyay, Rajour Tanyi Ako, Nicholas P. Lawrence, Jakeya Sultana, Abhishek Ranjan, Brian Wai-Him Ng, Nelson Tansu, Madhu Bhaskaran, Sharath Sriram, and Derek Abbott

The study of optical resonators is of significant importance in terms of their ability to confine light in optical devices. A major drawback of optical resonators is the phenomenon of light emission due to their limited capacity for light confinement. Bound states in the continuum are gaining significant attention in the realization of optical devices due to their unique ability for reducing light scattering via interference mechanisms. This process can potentially suppress scattering, leading to improved optical performance. Using this concept, a metasurface having two elliptical silicon (Si) resonators nonidentically angled to create an out-of-plane asymmetry is studied. Various parameters are optimized by employing a genetic algorithm (GA) to subsequently achieve a high-*Q* factor at terahertz frequencies. Herein, the device is fabricated using a novel method, and a thick high-index resonator is achieved. Terahertz measurements are carried out to validate the results. It is indicated in the experimental results that plasmons appear at the top surface of the metasurface and create strong sharp resonances that are sensitive to the external environment. Owing to strong field confinement ability, and high-*Q* factor, the metasurface is sensitive to its surrounding environment and can be essentially employed in terahertz sensing applications.

1. Introduction

The emerging concept of dielectric metasurfaces demonstrates a low-loss system for effective control and sub-wavelength manipulation of electromagnetic waves. These metasurfaces are an emerging topic in the field of nanophotonics due to their potential for producing high-*Q* factor resonances. Significant advances in meta-photonics have led to the propagation of unconventional electromagnetic modes known as bound states in the continuum (BICs). It is known that BICs can be efficiently used to prevent scattering loss and constrain light within the continuum.[1–3] Notably, BICs provide a simple and unique interference mechanism for primarily achieving high-*Q* factors and light–matter interaction in dielectric metasurfaces, which is mainly achieved through excitation of super-cavity modes.[3,4] The existence of BIC states is due to the interference of waves in the system. The wave functions associated with the continuum states interfere destructively with the wave function of the bound state at a particular energy, resulting in a cancellation of the outgoing waves. As a result, the bound state remains localized and does not couple to the continuum, even though it has the same energy as the continuum states.

Metasurfaces made from high-index resonant dielectrics have emerged as an essential building block because of their low intrinsic losses and unique light control capability. The use of high-index dielectrics increases light localization on the surface that is extremely sensitive to external environments.[2,5] To achieve a high-*Q* factor in the optical regime, several approaches have been reported in the literature by different research groups.[6–13] However, achieving high-*Q* factors in the terahertz regime remains an active and challenging research problem.

In 2011, Jansen et al.[14] reported an experimental study with an asymmetric split ring resonators achieving a *Q* factor of 30 within the 0.2–0.4 THz range. An ultrasensitive refractive index metasurface sensor was proposed by Singh et al., showing that the Fano resonance of the metasurface can also attain high-*Q*

M. S. Islam, N. P. Lawrence, J. Sultana, B. W. H. Ng, N. Tansu, D. Abbott
School of Electrical and Mechanical Engineering
The University of Adelaide
Adelaide, SA 5005, Australia
E-mail: mdsaiful.islam@adelaide.edu.au

The ORCID identification number(s) for the author(s) of this article can be found under https://doi.org/10.1002/adpr.202300121.

M. S. Islam, N. Tansu
Institute for Photonics and Advanced Sensing (IPAS)
The University of Adelaide
Adelaide, SA 5005, Australia

A. Upadhyay, R. T. Ako, M. Bhaskaran, S. Sriram
Functional Materials and Microsystems Research Group
RMIT University
Melbourne, Victoria 3001, Australia

A. Ranjan
School of Engineering
Sapienza University of Rome
Pizzale Aldo Moro, 00185 Roma, Italy

**ADVANCED
SCIENCE NEWS**

www.advancedsciencenews.com

**ADVANCED
PHOTONICS
RESEARCH**
Open Access

www.adpr-journal.com

factors.[15] Using Fano resonance on a metallic metasurface, Srivastava et al. obtained an improvement in Q factor.[16] These works demonstrate that at terahertz frequencies, the Q factor of a metasurface is extremely sensitive to metallic conductive properties and geometries. Recently, Han et al.[17] demonstrated a symmetry-broken-transmissive high-Q all dielectric metasurface exploiting extended BICs. Further experimental study on the silicon cross structure demonstrated a maximum Q-factor of around 70. In 2020, Kyaw et al.[4] demonstrated two distinct methodologies for driving BICs at terahertz frequencies, the first by linear polarization of light for symmetric-protected BICs and the second by using capacitive-mediated coupling for Friedrich–Wintgen BICs. With an asymmetric metasurface structure, a Q factor of 23.7 was achieved. A new dynamic modulation technique is demonstrated by Li et al. to control metal metasurfaces supporting BICs or quasi–BICs. Introducing graphene on a metal surface and taking advantage of graphene's electron concentration, both BIC and quasi-BIC modes were demonstrated.[18] The terahertz metasurfaces discussed earlier[4,14–19] all show promising characteristics, yet there remains scope to propose new metasurface devices that can achieve high-Q factors.

In this article, we demonstrate a BIC-enabled high-Q silicon metasurface having a pair of elliptical structures on the top surface. Then parametric optimization is carried out using a genetic algorithm (GA), targeting sharp resonance in the terahertz regime. The simulation results show that the metasurface can achieve a high-Q factor of approximately 4200, with an absorption approaching unity. The metasurface is fabricated using a novel and unconventional fabrication method. After the first fabrication trial, we resimulate the structure considering the dimensions achieved after fabrication. With these modified dimensions, simulation results show a Q factor of approximately 950, and the subsequent experimental outcome shows a Q factor of around 250. The resonance frequency in the experiment is reasonably matched with simulation, with the difference accountable by thickness variation in the fabricated structure that is addressable by future refinement. The reported metasurface exhibits strong field enhancement at each silicon ellipse making it suitable for refractive index sensing applications.

2. Design, Simulation, and Fabrication

The design and simulation of the proposed metasurface is carried out via the CST Studio Suite. A frequency-domain solver, and tetrahedral mesh type is adopted in the simulation. In a Floquet port boundary condition, the unit cell is defined in the x–y direction and the open add space in the z-direction. Details of boundary conditions and mesh type are extensively discussed in our previous publication.[20] In order for the metasurface to function as a reflector, metallic gold is considered as a perfect electric conductor (PEC)-type material. The frequency-dependent permittivity of gold can be derived from[21]

$$\varepsilon(\omega) = \varepsilon_\infty - \frac{\omega_p^2}{\omega^2 + i\omega\gamma} \qquad (1)$$

where ε_∞ is the permittivity at infinite frequency, ω_p is defined as plasma frequency, and γ represents the collision frequency. These values for ε_∞, ω_p, and γ are 1.0, 1.38×10^{16} rad s^{-1}, and 1.23×10^{13} s^{-1}, respectively.[21]

The schematic of the metasurface, including signal direction, is shown in **Figure 1**. On top of the gold reflector, cyclic olefin copolymer (COC) is chosen as a dielectric material because of its low loss, and high chemical and thermal stability at terahertz frequencies. The dielectric constant of COC is taken from the recent experimental study on materials.[22] The dielectric constant and loss tangent of SU-8 is taken as 2.92 and 0.055, respectively.[23] The elliptical patterns at the top surface are made by high-resistivity silicon (HR-Si) whose dielectric constant and loss tangent is taken as 11.68 and 0.00002, respectively.[24] The unit cell of the metasurface includes two elliptical resonators where one is angled by 6° with respect to the other. The optimization of the metasurface is carried out using the GA optimization tool built into CST Studio. The desired goal is to minimize the reflection coefficient S_{11}, so that maximum absorption can be obtained
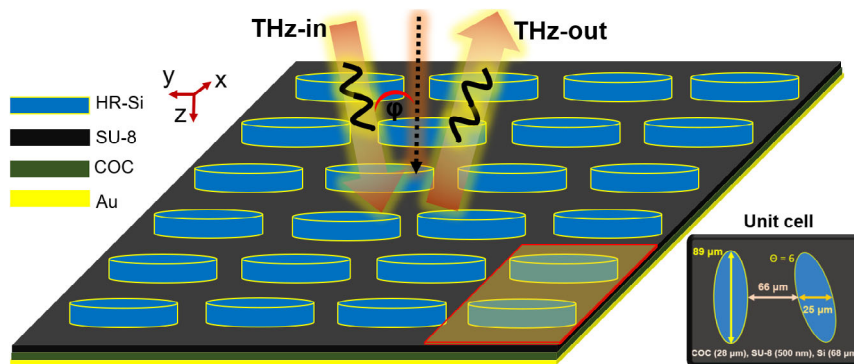
Figure 1. Schematic of the metasurface under study, indicating the materials used, the patterning, and the unit cell. The arrows on top of the metasurface indicate the incoming and outgoing beam directions at the metasurface. The unit cell also shows the dimension of the optimized metasurface. The material gold (Au) is used as a ground plane, cyclic olefin copolymer (COC) is chosen as the substrate due to its desirable characteristics at terahertz frequencies, and SU-8 is used as an adhesive material to improve adhesion between COC and Si. The schematic diagram indicates an incoming electromagnetic signal from the terahertz transmitter. This signal is subsequently manipulated at the metasurface before being reflected back toward the terahertz receiver.

for the desired frequency. Our focus is to achieve a sharp resonance peak so that a high-Q factor can be achieved.
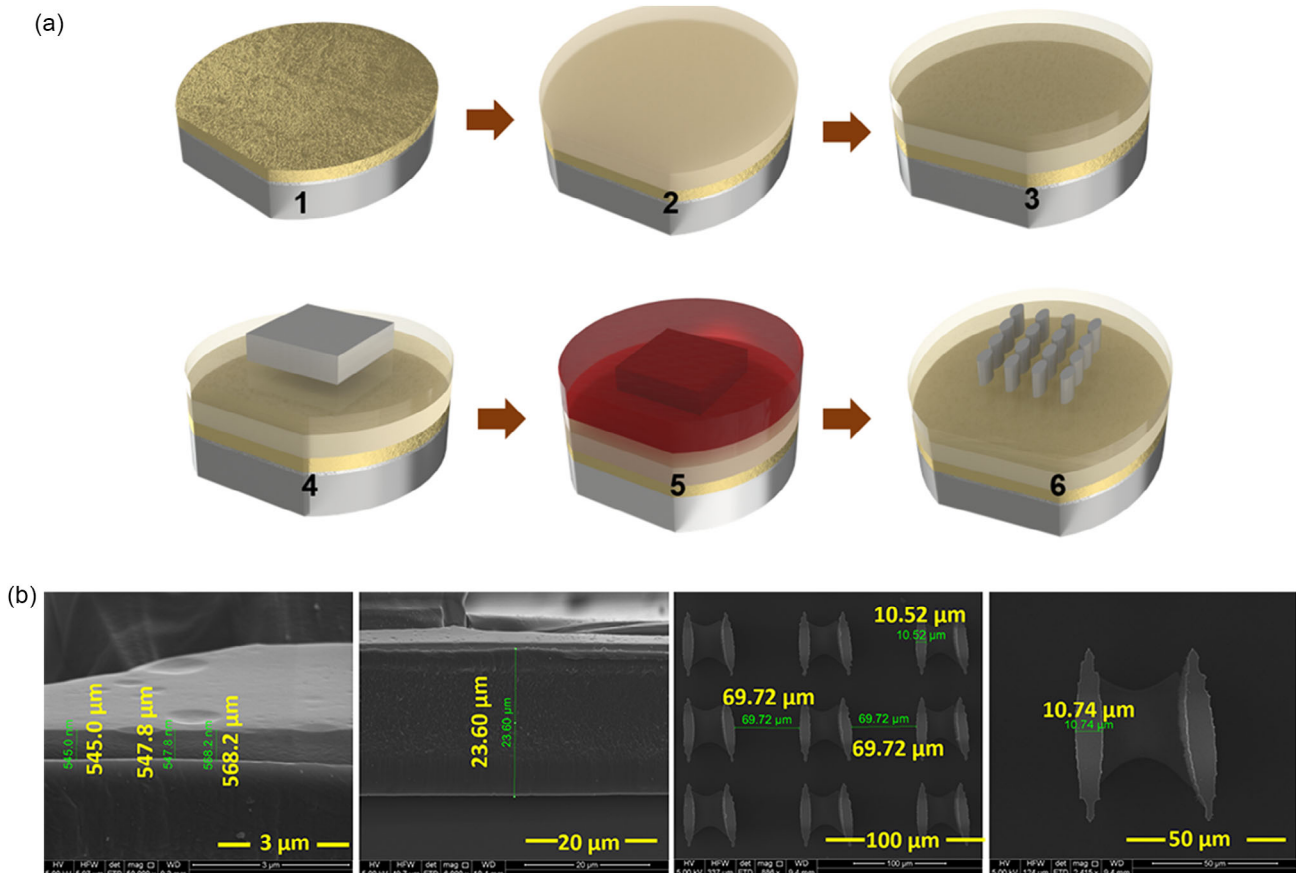
2.1. Fabrication

To fabricate the initial metasurface, an unconventional fabrication technique to realize HR-Si resonators on a COC polymer film is employed. To our knowledge, this is the first time that HR-Si on polymer has been placed on top of COC. The fabrication procedure is novel yet challenging. The first challenge is to successfully bond HR-Si to the dielectric material (COC). Here, SU-8 2000.5 is used for this crucial step. Note that COC is chosen as the dielectric for its low loss across the entire terahertz range. Additionally, COC has a constant refractive index over a wide wavelength range, and is capable of being spun to various thicknesses, which brings flexibility to the fabrication process.[22] The next challenge is to etch down the silicon until the desired height of resonators is achieved. This is achieved through a very slow and controlled plasma etching of the sample using deep reaction ion etching (DRIE) process. This is carried out carefully as heat generation during the etching process may weaken the bonding between SU-8 and the HR-Si layer, thus leading to silicon liftoff. Considering the use of special materials,

such as COC and HR-Si, the standard fabrication methods are unsuitable for the proposed device. Hence, the need for our unconventional and novel fabrication approaches to realize this all-dielectric high-Q metasurface.

As indicated in **Figure 2**a, the fabrication steps include polymer film coating, wafer to polymer film bonding, plasma etching, standard photolithography for patterning, and DRIE, respectively. First, a metallic ground plane composed of chromium/gold (Cr/Au), with thicknesses 20/200 nm, respectively, is deposited on a 3 inch Si wafer using electron beam deposition (PVD75, Kurt J. Lesker). Then COC (mr–I T85–20) is then spin-coated on the Au ground plane (Laurell spinner 650 M) at 2500 rpm for 30 s. The COC layer is dehydrated on a hot plate by ramping the temperature to 95 °C for 10 min and then to 120 °C for 20 min. The COC thickness, on another wafer using the same process, is calibrated with a stylus profilometer to be $t = 27 \pm 1\,\mu m$. Next, SU-8 is spin-coated on the metal-backed COC layer at 3000 rpm for 30 s to achieve the desired thickness of 500 nm. This SU-8 layer is then treated with flood UV exposure for 5 s.

The HR-Si wafer is then attached to the COC using SU-8 as an adhesive layer. Thereafter, HR-Si is etched to a thickness equivalent to height of resonators. To realize the resonators, standard

(a)

(b)

Figure 2. Fabrication of the metasurface. a) Step-by-step metasurface fabrication procedure, b) scanning electron microscopy images of the fabricated samples showing the obtained SU-8 thickness, COC thickness, the unit cell, and the metasurface array. While we are able to achieve the desired thicknesses of COC and SU-8, considerable variation in Si resonator thickness was observed. This resulted in some divergence between simulated and experimental outcomes.

photolithography is exploited to create a hard mask on the HR-Si surface. A thick layer of photoresist is achieved by spinning AZ4562 at 2000 rpm, for 30 s, followed by a soft bake at 95 °C for 90 s. Maskless photolithography (MLA150 Maskless Aligner, Heidelberg Instruments) is used to pattern the elliptical resonators. This sample is then developed using a mixture of AZ-400 K and deionized water, in a 1:2 ratio. The patterned substrate is then hard baked at 120 °C for 2 h.

A second plasma etching is carried out in a DRIE tool (Oxford Instrument PLASMA-LAB-100 ICP-380). A standard silicon BOSCH DRIE process is used. After the etching, the residual photoresist is stripped off using an oxygen-only clean recipe in the plasma chamber. Finally, the height of the ellipses is characterized through profilometer (3D Optical profiler-Contour GT-Bruker) and high-resolution scanning electron microscope.

3. Results and Discussion

3.1. Reflection and Absorption

The simulation is carried out for two different dimension sets of the metasurface: one dimension set includes optimized parameters while the other set includes dimensions achieved after fabrication. **Figure 3**a shows the reflection and absorption properties for the optimized parameters, indicating a sharp resonance at 1.308 THz, with unity absorption, high reflection, and zero transmission observed. Transmission is negligible as the metasurface is a reflector with a metal-backed substrate. Importantly, the achieved Q factor is around 4200, which is extremely high and rarely achieved at terahertz frequencies. Moreover, this is the first time we have fabricated such a high-Q metasurface structure using this novel fabrication technique. Figure 3b shows the reflection and absorption of the metasurface having the dimensions achieved after fabrication, indicating an absorption >90%. With the actual fabricated dimensions, the resonance frequency is slightly shifted to around 1.303 THz with the simulated Q factor being around 900.

3.2. Mechanism behind the Plasmon Enhancement and Sharp Resonance

The proposed metasurface shown in Figure 1 consists of HR-Si patterned on top of an adhesive SU-8 material. A polymer COC substrate lies below resting on a metal ground plane. To explore the science behind the strong surface plasmons, we show different mode fields including E-field, H-field, power loss density, and surface current shown in **Figure 4**. We see that the mode fields are strongly confined to the Si resonators—one reason is the high refractive index while the other is the optimized dimensions and asymmetry of the of Si resonators. The excitation of the plasmonic mode occurs when the photons from the incident electromagnetic wave interact with the Si resonators of near sub-wavelength dimensionality. At the resonance frequency, the incoming electromagnetic energy is strongly coupled and dissipated in the high-index Si and the other polymer substrate due to the dielectric loss. This results in the absorption of energy at the resonance frequency. For the cases of multiband absorbers, some of the photons usually reflect from the substrate or eventually from the metal reflector, creating subsequent plasmons. Led by destructive interference of the reflected photons, the process repeats multiple times until zero reflection occurs.[20] Due to the metallic reflector, the transmitted energy through the sample is zero. At frequencies other than the resonant frequency, the incident electromagnetic wave is reflected and no energy is absorbed. Evidence in support of the previous discussion can be found from Figure 4. Figure 4a,b indicates that the electromagnetic energy in the form of electric and magnetic fields are strongly concentrated in the resonator with orthogonality between these fields demonstrated. This strong field confinement in the high-index Si resonator is an indicator of strong plasmons and sharp resonance at the frequency of operation. Moreover, the power loss density, as shown in Figure 4c, is indicative of strong coupling of the electromagnetic field at the resonator. The surface current, as shown in Figure 4d, indicates that the currents are concentrated at the metallic ground plane indicating reflection of incoming photons.
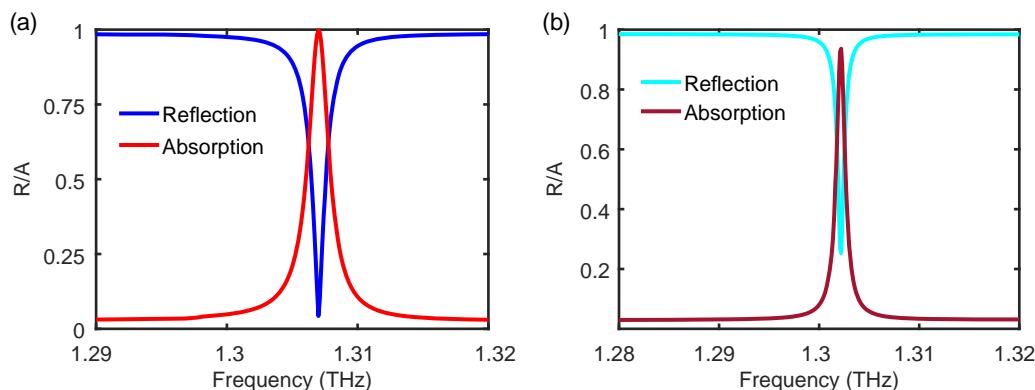
Figure 3. Simulated reflection and absorption spectra of the metasurface: a) using the optimized dimensions of the materials achieved through a genetic algorithm; b) using the obtained feature dimensions after fabrication. Both plots show strong absorption near unity with a sharp resonance peak around 1.3 THz indicating a high-Q factor.
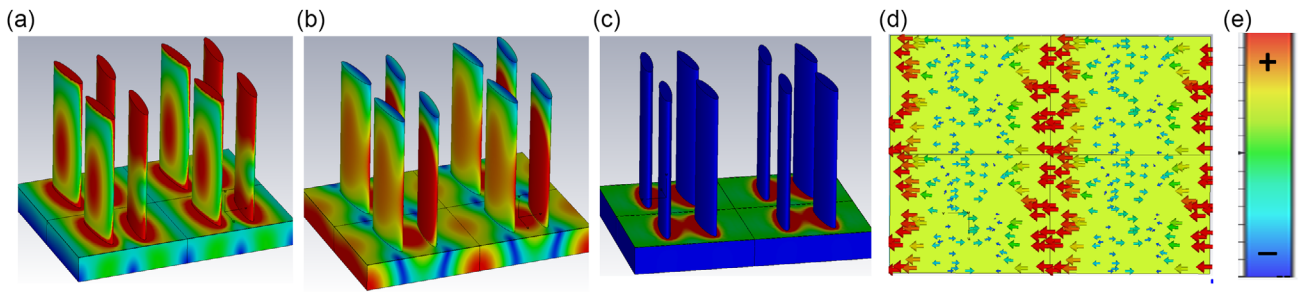
Figure 4. Electromagnetic field distribution: a) electric field, b) magnetic field (orthogonal to the electric field), c) power loss density, d) surface current, and e) generalized color bar for figure (a–d). The optimized dimensions of the metasurface are considered in generating the field distribution profile. Illustrating strong field confinement adjacent to silicon resonator desired for sensing.

### 3.3. Parameter Tuning and BIC

Further insight into plasmon enhancement and sharp resonance is demonstrated in **Figure 5**. Reflection varies as a function of Si resonator angle and thickness, as observed. Starting from the ellipse angle, it can be seen in Figure 5a that at an ellipse angle of 0°, with all other parameters optimized, at the metasurface demonstrates a Q factor of 757. However, increasing the asymmetry by changing the ellipse angle up to 6° increases the Q factor. Beyond this value of ellipse angle, with all other parameters optimized, destructive interference in the metasurface occurs creating a BIC mode with the highest field confinement and sharpest resonance. This leads to the highest Q factor in the case of optimized dimensions of the metasurface of around 4200. The contour plot of Figure 5c provides evidence of maximum reflection at an ellipse angle

of 6°–demonstrating the existence of a BIC operational mode in the metasurface.
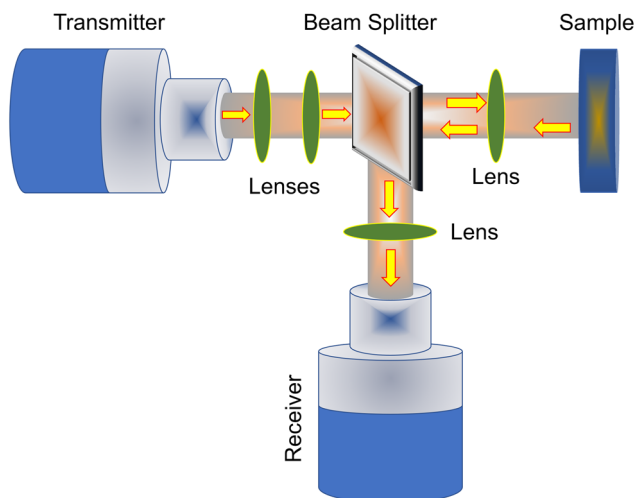
In a similar fashion, but instead of changing the Si thickness, the performance variation of the metasurface in consideration of sharp resonance is shown in Figure 5b. Keeping the ellipse angle constant at 6° along with other optimized parameters, a Si thickness of 64 μm provides a Q factor of 1458. The thickness is then optimized at 67 μm, enhancing the plasmon creation at the resonators, creating a sharp resonance, and increasing the Q factor. The contour plot of Figure 5d demonstrates a maximum electromagnetic field confinement at 67 μm.

3.4. Experimental Analysis

We carry out the experiment using the Advantest Terahertz System (TAS7400TS), and further validate the results by
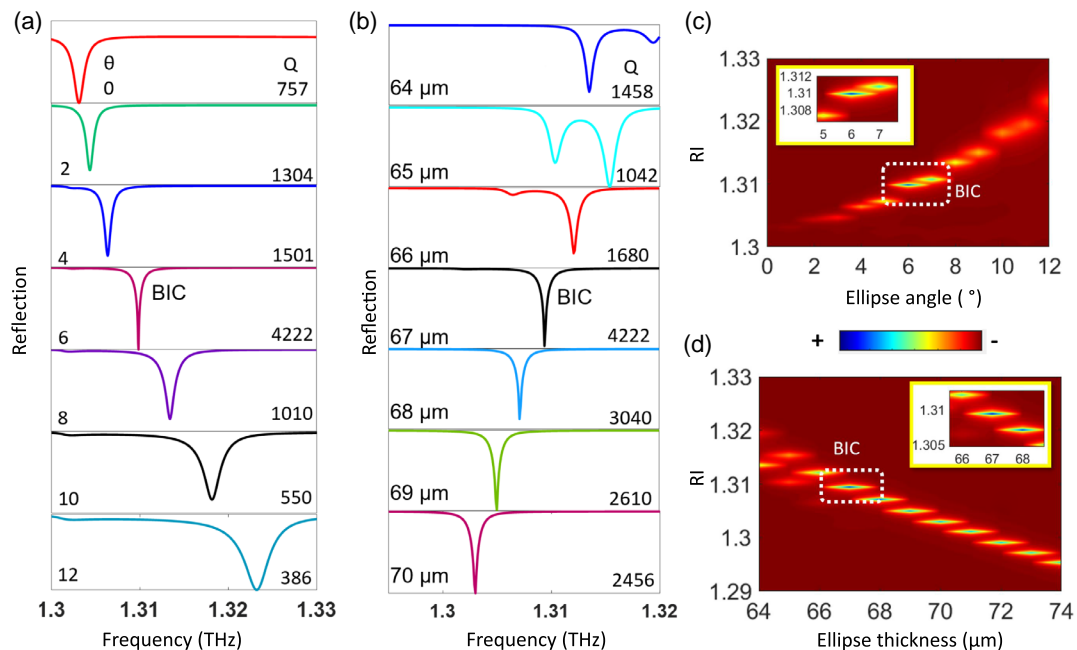
Figure 5. The reflection coefficient and Q factor of the metasurface: a) changing the elliptical resonator angle when keeping other parameters optimized demonstrates a bound states in the continuum (BIC) mode formed at 6°, indicating the sharpest resonance and highest Q factor, b) keeping the elliptical angle and other parameters constant but changing the resonator thickness indicates the BIC mode occurring at 67 μm, c,d) maximum reflection at 6° angle, and at 67 μm thickness, of the resonator respectively, forming the BIC mode and achieving the highest Q factor.

**ADVANCED
SCIENCE NEWS**

www.advancedsciencenews.com

**ADVANCED
PHOTONICS
RESEARCH**
Open Access

www.adpr-journal.com

Figure 6. Experimental setup for the metasurface measurement. Showing the standard setup using the Menlo system whereas an identical setup without lenses is used for the Advantest terahertz system.

experimentation using the Menlo system (TERA K15). We find the Q-factor obtained using the TAS7400TS closely matches that obtained with the TERA K15. However, a slight difference in resonance frequency does occur and this may be due to alignment mismatch and the location of the metasurface where the incident beam excites the metasurface. The experimental setups for both systems are shown in **Figure 6**. In both setups, we employ a beam splitter, as the metasurface is designed to work at normal incidence angle ($\phi = 0°$).

In case of the Advantest system, as shown in Figure 6a, we achieve the required beam profile for carrying out the experiment without using any further lenses or parabolic mirrors. We are able to achieve a sampled signal bandwidth of around 3.0 THz, as the achievable bandwidth with the system is around 4.0 THz. In the case of the Menlo system, we use lenses to achieve the required beam profile. Using our current Menlo system, we can achieve a maximum bandwidth of 2.0 THz, and the 1.3 THz resonance frequency is well within this limit.

Using the Advantest and Menlo systems, the amplitude and power of the reference and sample signal and the normalized

power are shown in **Figure 7**. The reference signal is taken by replacing the sample with a gold coated mirror, acting as a reflector. From the time–domain signal, it can be seen that there is a considerable amount of shift from the reference signal to sample signal in signal amplitude unit over time (ps). This is due to the losses incurred by the whole structure. From the frequency domain signal–achieved after performing an FFT on the time domain signal–it can be seen that although we can achieve a free space bandwidth of around 4.0 THz, in practice, a usable bandwidth of around 3.0 THz is achieved when the sample is inserted. This is due to the losses occurred, when the terahertz signal is incident on the sample's surface, travelling through the sample's layers, and reflecting back from the ground plane

From the reflection plot in Figure 7, it is clear that there is a sharp resonance peak at around 1.3 THz, which is a close match with the simulation result considering the obtained dimensions after fabrication, as shown in Figure 3b. In a more precise measurement, we find the simulated resonance frequency at 1.303 THz with a slight shift in experimental resonance frequency to 1.301 THz. With this shift being insignificant, simulated and experimental outcomes are in close agreement.

The Q factor obtained in the experiment is 236, which is calculated by taking the center frequency and dividing it by full width at half maxima, and is comparable to recent reports.[4,14,16,17,25–27] From the experimental outcome shown in Figure 7, we can see the reflection from the metasurface is very low and therefore the absorption of the metasurface is close to unity.

4. Discussion

Despite promising results in simulated and experimental resonance frequencies, discrepancies exist in the measured Q factor. Various reasons for these discrepancies are given later. One reason is dependency on the array size where previous experiments have shown that the Q factor of a metasurface increases as a function of array size.[28] Therefore, if we fabricate the metasurface with an increased array size, the Q factor can be increased. The second reason can be due to imperfect fabrication of the metasurface. In the fabrication of large arrays, the probability of undesired liftoff of silicon increases. These added
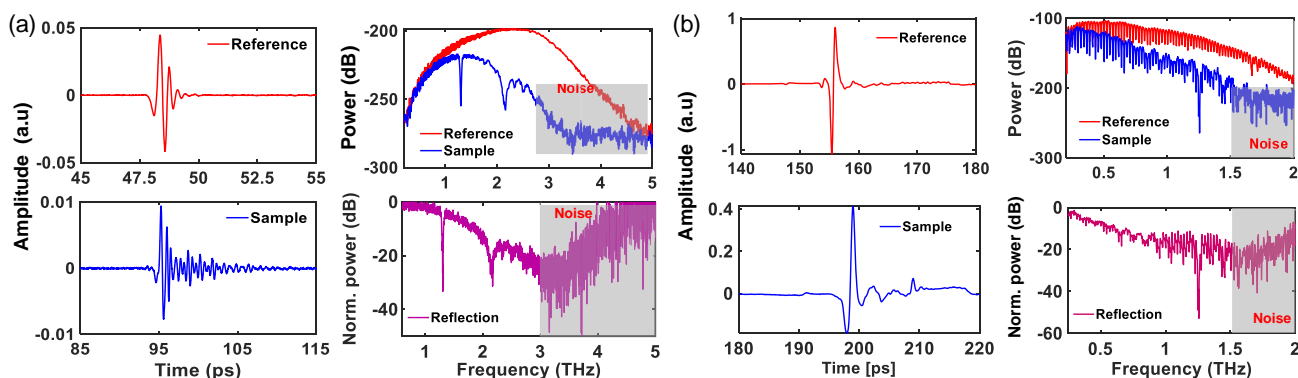
Figure 7. Experimental outcome of the metasurface using both the Advantest and Menlo systems. a) Amplitude, reflected power from the sample and reference, and the normalized power of the metasurface using the Advantest terahertz system, demonstrating a sharp resonance at 1.301 THz. b) The same experiment as in (a), but using the Menlo system, demonstrates a resonance frequency of 1.296 THz.

**ADVANCED
SCIENCE NEWS**

www.advancedsciencenews.com

**ADVANCED
PHOTONICS
RESEARCH**
Open Access

www.adpr-journal.com

imperfections may cause a reduction in the Q factor. Lastly, the Q factor might be limited due to additional measurement mismatch. For example, the imperfections with in collimation or other aspects of the measurement environment.

In this work, we have only considered elliptical silicon resonators for creating asymmetry in the structure before optimization to create strong plasmonic effects that are sensitive to the external environments. The resonance frequency of the metasurface is dependent on the material properties and their dimensions. For example, changing the thickness of COC or SU–8 can potentially change the resonance frequency. The Q factor of this kind of metasurface device can be further increased by more precise fabrication of the device.

In **Table 1**, we compare high-Q plasmonic metasurfaces. In addition to the Q factors, we have also included other relevant results, such as operating frequency, the material used to create plasmons, and physical mechanism used to confine electromagnetic fields on the metasurface. From the table, the center frequency of most of the metasurfaces is below 1.0 THz. One possible reason for this observation may be due to the availability of terahertz systems and specifically the operating frequencies they can readily provide. Indeed, one possible advantage of making the metasurface operate at these lower terahertz region (<1 THz) is the availability of terahertz systems to carry out experiments at lower frequencies. A perfect alignment of the Menlo system we have in our lab can provide an operating frequency from 0.2 THz to a maximum of 2.0 THz, while the Advantest system can provide an operating frequency within the range of 0.4–5.0 THz. In our case, as we have both sets of equipment for carrying out experiments above 1.0 THz, so a lower terahertz region operational restriction did not affect our experimentation.

Metallic resonators are a common platform for plasmonic metasurfaces.[4,14,16,25,26] However nowadays high-indexed dielectric resonators provide promising outcomes in terms of loss and Q factor.[17,27] In our case, we used a high-index Si to achieve a high-Q factor. The obtained Q factor is comparable with recent experimentally obtained outcomes.[4,14,16,17,25–27]

To summarize, we have fabricated and experimentally demonstrated a BIC-enabled high-Q terahertz plasmonic metasurface, demonstrating reasonable agreement with the simulation results using actual fabricated dimensions. Our work presents a

promising outcome in terms of Q factor when compared with relevant literature. We have found that the observed Q factor obtained from the simulation may be limited by the array size, fabrication issues, and the experimental environment. Additionally, our metasurface follows a simple yet novel design principle and can be tuned to operate over a range of frequencies, as well as be tuned to operate at multiple resonances. The proposed metasurface highlights the potential of high-index dielectrics for achieving high-Q factor and expands the capabilities of BIC-enabled plasmonic metasurface for various photonic applications.

Conflict of Interest

The authors declare no conflict of interest.

Author Contributions

M.S.I. conceived the idea, carried out simulation and the experiments; A.U., and R.T. Ako carried out the fabrication; M.S.I. and A.U. wrote the article. All authors checked, discussed, analyzed, and interpreted the results. The manuscript was proof read and corrected by all the authors; M.B. and S.S. supervised the fabrication work; B.W.-H.N. and D.A. supervised the overall study; D.A., S.S., and N.T. approved the final submission of the manuscript.

Open access publishing facilitated by The University of Adelaide, as part of the Wiley - The University of Adelaide agreement via the Council of Australian University Librarians.

Data Availability Statement

The data that support the findings of this study are available on request from the corresponding author. The data are not publicly available due to privacy or ethical restrictions.

Table 1. Summary of experimentally obtained Q factors for comparable metasurfaces and a comparison with our proposed metasurface.

References	Frequency [THz]	Q factor	Material	Mechanism
[14]	0.5	31	Au	D-split ring resonator
[16]	0.53	50	Al	Fano resonance
[17]	0.95	109	Si	Quasi-BIC
[4]	0.6	25	Ag	Quasi-BIC
[25]	0.69	11.6	Al-NP	Metal plasmonics
[26]	0.81	58	Au	Fano resonance
[27]	0.53	70	Ge	Quasi-BIC
[29]	0.53	100	Al	Quasi-BIC
This work	1.3	236	Si	BIC

Keywords

[1] K. Koshelev, Y. Kivshar, *Nature* **2019**, *574*, 491.
[2] C. W. Hsu, B. Zhen, A. D. Stone, J. D. Joannopoulos, M. Soljacic, *Nat. Rev. Mater.* **2016**, *1*, 16048.
[3] M. Rybin, Y. Kivshar, *Nature* **2017**, *541*, 164.

**ADVANCED
SCIENCE NEWS**

www.advancedsciencenews.com

**ADVANCED
PHOTONICS
RESEARCH**
Open Access

www.adpr-journal.com

[4] C. Kyaw, R. Yahiaoui, J. A. Burrow, V. Tran, K. Keelen, W. Sims, E. C. Red, W. S. Rockward, M. A. Thomas, A. Sarangan, I. Agha, T. A. Searles, *Commun. Phys.* **2020**, *3*, 212.

[5] A. I. Kuznetsov, A. E. Miroshnichenko, M. L. Brongersma, Y. S. Kivshar, B. Lukyanchuk, *Science* **2016**, *354*, 6314.

[6] S. Campione, S. Liu, L. I. Basilio, L. K. Warne, W. L. Langston, T. S. Luk, J. R. Wendt, J. L. Reno, G. A. Keeler, I. Brener, M. B. Sinclair, *ACS Photonics* **2016**, *3*, 2362.

[7] A. Leitis, A. Tittl, M. Liu, B. H. Lee, M. B. Gu, Y. S. Kivshar, H. Altug, *Sci. Adv.* **2019**, *5*, eaaw2871.

[8] C. Sui, X. Li, T. Lang, X. Jing, J. Liu, Z. Hong, *Appl. Sci.* **2018**, *8*, 161.

[9] K. Koshelev, S. Lepeshov, M. Liu, A. Bogdanov, Y. Kivshar, *Phys. Rev. Lett.* **2018**, *121*, 193903.

[10] J. F. Algorri, D. C. Zografopoulos, A. Ferraro, B. García-Cámara, R. Beccherelli, J. M. Sánchez-Pena, *Opt. Express* **2019**, *27*, 6320.

[11] X. Wang, J. Duan, W. Chen, C. Zhou, T. Liu, S. Xiao, *Phys. Rev. B* **2020**, *102*, 155432.

[12] S. Xiao, M. Qin, J. Duan, F. Wu, T. Liu, *Phys. Rev. B* **2022**, *105*, 195440.

[13] X. Chen, Y. Zhang, G. Cai, J. Zhuo, K. Lai, L. Ye, *Nanophotonics* **2022**, *11*, 4537.

[14] C. Jansen, I. A. I. Al-Naib, N. Born, M. Koch, *Appl. Phys. Lett.* **2011**, *98*, 051109.

[15] R. Singh, W. Cao, I. Al-Naib, L. Cong, W. Withayachumnankul, W. Zhang, *Appl. Phys. Lett.* **2014**, *105*, 171101.

[16] Y. K. Srivastava, M. Manjappa, L. Cong, W. Cao, I. A. Naib, W. Zhang, R. Singh, *Adv. Opt. Mater.* **2016**, *4*, 457.

[17] S. Han, P. Pitchappa, W. Wang, Y. Kumar, S. Mikhail, V. R. Singh, *Adv. Opt. Mater.* **2021**, *9*, 2002001.

[18] J. Li, C. Zheng, Z. Yue, S. Wang, M. Li, H. Zhao, Y. Zhang, J. Yao, *Carbon* **2021**, *182*, 506.

[19] S. Han, L. Cong, Y. K. Srivastava, B. Qiang, M. V. Rybin, A. Kumar, R. Jain, W. X. Lim, V. G. Achanta, S. S. Prabhu, Q. J. Wang, Y. S. Kivshar, R. Singh, *Adv. Mater.* **2019**, *31*, 1901921.

[20] M. S. Islam, J. Sultana, M. Biabanifard, Z. Vafapour, M. J. Nine, A. Dinovitser, C. M. B. Cordeiro, B. W.-H. Ng, D. Abbott, *Carbon* **2020**, *158*, 559.

[21] Z. H. Zhu, C. C. Guo, K. Liu, W. M. Ye, X. D. Yuan, B. Yang, T. Ma, *Opt. Lett.* **2012**, *37*, 698.

[22] M. S. Islam, J. Sultana, C. M. B. Cordeiro, M. J. Nine, A. L. S. Cruz, A. Dinovitser, B. W.-H. Ng, H. E. Heidepriem, D. Losic, D. Abbott, *IEEE Access* **2020**, *8*, 97204.

[23] N. Ghalichechian, K. Sertel, *IEEE Antennas Wirel. Propag. Lett.* **2015**, *14*, 723.

[24] J. Dai, J. Zhang, W. Zhang, D. Grischkowsky, *J. Opt. Soc. Am. B* **2004**, *21*, 1379.

[25] L. Cong, S. Tan, R. Yahiaoui, F. Yan, W. Zhang, R. Singh, *Appl. Phys. Lett.* **2015**, *106*, 031107.

[26] Q. Xie, G.-X. Dong, B.-X. Wang, W.-Q. Huang, *Nanoscale Res. Lett.* **2018**, *13*, 294.

[27] T. C. Tan, Y. K. Srivastava, R. T. Ako, W. Wang, M. Bhaskaran, S. Sriram, I. Al-Naib, E. Plum, R. Singh, *Adv. Mater.* **2021**, *33*, 2100836.

[28] M. S. Bin-Alam, O. Reshef, Y. Mamchur, M. Z. Alam, G. Carlow, J. Upham, B. T. Sullivan, J.-M. Menard, M. J. Huttunen, R. W. Boyd, K. Dolgaleva, *Nat. Commun.* **2021**, *12*, 974.

[29] L. Cong, R. Singh, *Adv. Opt. Mater.* **2019**, *7*, 1900383.